

# Water-Compatible Poly(methyl methacrylate) Networks for Visible Light-Driven Photocatalytic Pollutant Remediation in Aqueous Medium

Niklas Huber, Masis Sirim, Zhuangfei Qian, Calum T. J. Ferguson, Wenxin Wei, and Kai A. I. Zhang\*

Cite This: *ACS Appl. Polym. Mater.* 2022, 4, 5728–5736

Read Online

ACCESS |



Metrics &amp; More



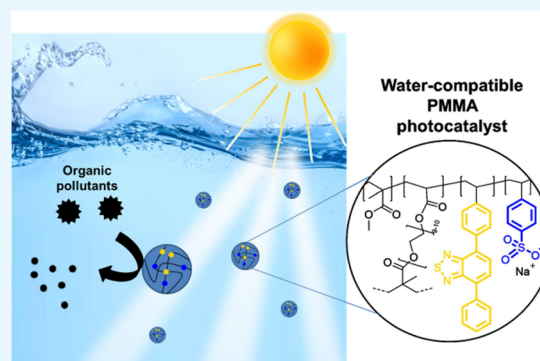
Article Recommendations



Supporting Information

**ABSTRACT:** Using polymeric photocatalytic materials for visible light-driven heterogeneous conversion of organic substances in environmentally benign reaction media as in water, in particular, has gained much attention recently. Most of the current conjugated polymer photocatalysts are often unsuitable for applications in water because of their highly hydrophobic nature. Classical polymer-based photocatalysts possess advantages that include precise control of properties through facile synthesis and direct access to the toolbox of classical polymer chemistry. However, the effect of monomer composition remains unclear, and a systematic investigation of structure–property relationships is still missing. In this work, we design water-compatible poly(methyl methacrylate) (PMMA)-based polymer photocatalysts by precise control of comonomers with specific functions. The electronic and optical properties and water compatibility of PMMA photocatalysts could be tuned, and they showed direct dependence on the monomer composition. Mathematical as well as density functional theory simulation as hydration enthalpy calculations supported the observed effects. The photocatalytic degradation of 2,4-dichlorophenol in water as model reaction showed an optimum of polymer composition and solubility for the photocatalytic reactivity. More remediation of important contaminants was successfully conducted as diethyl phthalate, acetophenone, and bisphenol-A, which are common products from plastic degradation detected in groundwater.

**KEYWORDS:** heterogenous photocatalysis, toxic pollutant degradation, hydrophilic polymer, water treatment, radical polymerization, poly(methyl methacrylate)



## INTRODUCTION

The use of visible light for conversion of organic substances is an environmentally friendly alternative to conventional chemical reaction conduction by heat. Among the photocatalytic materials commonly used, pure organic polymer-based heterogeneous photocatalysts have recently received much attention.<sup>1–3</sup> Most of these polymer photocatalysts are fully conjugated polymer networks as conjugated microporous polymers, covalent triazine networks, covalent organic frameworks, and so forth.<sup>4–6</sup> A scarcely studied class of substances are photoactive classical polymers. They combine polymeric materials and photoactive small molecule properties by incorporating the latter as repeating units in a polymer backbone.<sup>7</sup> Their advantages include precise control of conjugation lengths, cost-effectiveness, chemical robustness, and variability of properties through facile synthesis and direct access to the toolbox of classical polymer chemistry.<sup>8,9</sup> A few studies undertaken to date showed their promising potentials in synthesis and photocatalytic applications but barely included systematic investigations of structure–property relationships.<sup>10–12</sup> In particular, the effect of monomer composition remains unclear. Such insights are essential to broaden

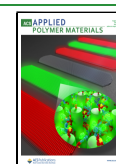
understanding and address the key challenge of designing photoactive classical polymer materials in the future.

A very attractive approach to use targeted material design for sustainable purposes is performing chemical reactions in green solvents.<sup>5</sup> Water, in particular, is a cheap, safe, and environmentally friendly alternative to organic solvents.<sup>13</sup> It is considered the preferred choice in practical applications concerning occupational safety, process safety, and environmental and regulatory aspects. Furthermore, the applicability of materials in aqueous medium opens several energy-, environmental-, and bioapplication-related possibilities, such as water splitting,<sup>14–16</sup> antibacterial treatment,<sup>17,18</sup> photodynamic therapy,<sup>19</sup> and water purification.<sup>3,20</sup> Given their usually fully aromatic backbone structure, conventional

Received: April 22, 2022

Accepted: July 20, 2022

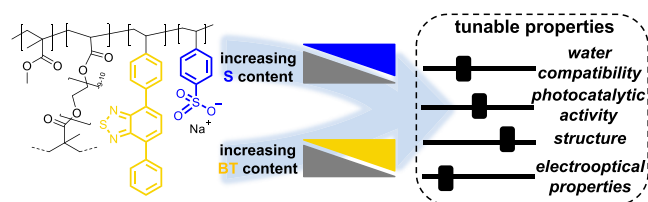
Published: July 28, 2022



polymer photocatalysts are often unsuitable for applications in water because of their highly hydrophobic nature. Moreover, the rigid bonds in conjugated networks tremendously hinder swelling by solvents and substrate diffusion. Previous modification strategies mainly included postsynthetic transformations,<sup>15,17,21</sup> surface functionalization,<sup>20,22,23</sup> or protonation by acids.<sup>24</sup> However, such synthesis methods are complex to perform and difficult to gain precise control.

In this work, we design water-compatible poly(methyl methacrylate) (PMMA)-based polymer photocatalysts by precise control of comonomers with specific functions (Scheme 1). The general effect of variable amounts of

### Scheme 1. Illustration of Molecular Design and Property Tuning by Varying the Photoactive Units Benzothiadiazole (BT) and Hydrophilic Comonomer Benzene Sulfonate (S) in Water-Compatible PMMA Photocatalysts



photoactive and water-mediating comonomers in the class of nonfully conjugated photocatalysts on structural, electro-optical, and photocatalytic properties was elucidated in detail. In particular, two series of cross-linked PMMA-based polymers were synthesized through radical polymerization. In **series 1**, the amount of photoactive moiety 4,7-diphenylbenzothiadiazole was gradually increased, and in **series 2**, the amount of solvent-mediating moiety 4-benzenesulfonate was gradually increased. The electronic and optical properties and water compatibility of the PMMA photocatalysts could be tuned and showed direct dependence on the monomer composition. Mathematical as well as DFT calculations supported the observed effects. Photocatalytic studies on the decomposition of organic pollutants showed the high activity of the polymers in aqueous medium. Kinetics of 2,4-dichlorophenol degradation in water showed an optimum of polymer composition and solubility for the photocatalytic reactivity. The reaction scope could be expanded to include the remediation of more contaminants as diethyl phthalate, acetophenone, and bisphenol-A, which are common products from plastic degradation detected in groundwater analyses.

## RESULTS AND DISCUSSION

**Synthesis and Structural Analysis.** The PMMA networks in this work were synthesized via free-radical polymerization from methyl methacrylate (MMA), polyethylene glycol dimethacrylate (PEGDMA), 4-phenyl-7-(4-vinylphenyl)-benzothiadiazole (BT), and sodium 4-vinylbenzenesulfonate (S). The synthesis was based on a previous literature report.<sup>25</sup> Details on synthetic procedures and comonomer ratios are given in the Experimental section and electronic supplementary information (ESI).

As listed in Table 1, in **series 1**, the molar content of BT was gradually increased from 0 to 50% (0, 2.5, 5, 10, 20, and 50). The amount of MMA was decreased accordingly, while PEGDMA (5%) and S (20%) were kept constant. The samples were denoted as BT<sub>0</sub>S<sub>20</sub>, BT<sub>2.5</sub>S<sub>20</sub>, BT<sub>5</sub>S<sub>20</sub>, BT<sub>10</sub>S<sub>20</sub>,

**Table 1. Compositional Overview of the Synthesized Photocatalytic PMMA Series<sup>a</sup>**

	series 1			
	PEGDMA	MMA	BT	S
BT <sub>0</sub> S <sub>20</sub>	5	75	0	20
BT <sub>2.5</sub> S <sub>20</sub>	5	72.5	2.5	20
BT <sub>5</sub> S <sub>20</sub>	5	70	5	20
BT <sub>10</sub> S <sub>20</sub>	5	65	10	20
BT <sub>20</sub> S <sub>20</sub>	5	55	20	20
BT <sub>50</sub> S <sub>20</sub>	5	25	50	20
	series 2			
	PEGDMA	MMA	BT	S
BT <sub>20</sub> S <sub>0</sub>	5	75	20	0
BT <sub>20</sub> S <sub>5</sub>	5	70	20	5
BT <sub>20</sub> S <sub>10</sub>	5	65	20	10
BT <sub>20</sub> S <sub>20</sub>	5	55	20	20
BT <sub>20</sub> S <sub>40</sub>	5	35	20	40

<sup>a</sup>Note: numbers are the molar percentage of the individual comonomers.

BT<sub>20</sub>S<sub>20</sub>, and BT<sub>50</sub>S<sub>20</sub>. In **series 2**, the molar content of S was gradually increased from 0% to 40% (0, 5, 10, and 40). Again, the amount of MMA was decreased accordingly, while PEGDMA (5%) and BT (20%) were kept constant. The samples were denoted as BT<sub>20</sub>-S<sub>0</sub>, BT<sub>20</sub>-S<sub>5</sub>, BT<sub>20</sub>-S<sub>10</sub>, and BT<sub>20</sub>-S<sub>40</sub>. Additionally, the sample BT<sub>20</sub>S<sub>20</sub> was suitable to be compared within **series 2**.

The synthesis of the polymers was confirmed by solid-state <sup>13</sup>C cross-polarization magic angle-spinning (CP-MAS) NMR spectroscopy. The signal intensities in the spectra can be used to estimate the ratios of the building blocks in the polymer. No double-bond signals are apparent in either series of the polymers. This indicates a high degree of polymerization and means that the reaction proceeded to completion. In cases where incompletely reacted vinyl monomers were present, purification by dialysis was successful. In **series 1** (Figure 1a),

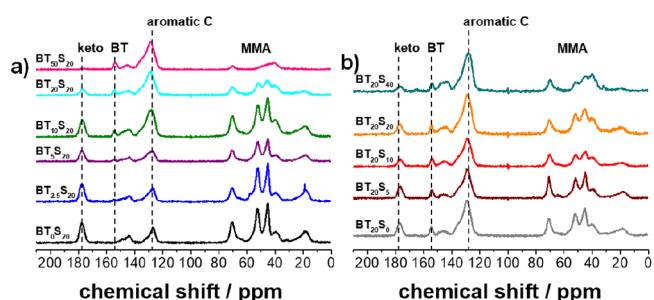


**Figure 1.** <sup>13</sup>C CP-MAS NMR spectra for (a) **series 1** with increasing BT and (b) **series 2** with increasing S content.

the signal of the keto group is observed at a chemical shift of 178 ppm. Further signals at 71, 52, 45, and 18 ppm can be assigned to the methyl and methoxy groups of MMA and the methylene backbone. All the signals of the MMA are in agreement with the literature values<sup>25</sup> and decrease within the series, which is in accordance with the decrease of the MMA content. The broad signal corresponding to the sulfonate unit (carbons in  $\alpha$ - and  $\delta$ -positions with respect to -SO<sub>3</sub>H) around 145 ppm is comparably constant. It can be observed that in the series from BT<sub>0</sub>S<sub>20</sub> to BT<sub>50</sub>S<sub>20</sub>, the BT-signal at 154 ppm emerges. In sample BT<sub>0</sub>S<sub>20</sub>, the BT signal is completely absent.

The broad signal around 128 ppm corresponds to aromatic carbons as it gets more pronounced when increasing the BT content. The number of aromatic carbons exceeds the number of MMA and backbone carbons to such an extent that the latter signals are strongly attenuated. The molar ratio trend can be confirmed in **series 1** with the spectra.

In **series 2** from BT<sub>20</sub>S<sub>0</sub> to BT<sub>20</sub>S<sub>40</sub>, the BT signal intensity is constant. In comparison, the S signals at 145 ppm increase within the series. This corresponds to the increase in sulfonate units and confirms the expected trend. As in **series 1**, the MMA and backbone signals become less prominent while the intensity of the phenylic carbon atoms increases. Both these effects are less pronounced than those in **series 1**, which is due to the lower C-atom excess in the benzenesulfonate vs the backbone compared to the three-membered aromatic BT.

Fourier-transformed infrared (FTIR) spectra were measured to further confirm the structural integrity of the polymers. Using the FTIR spectra of the vinyl monomers, bands were identified for normalization to a signal of the respective constant monomer (Figure S1, SI). Both series show no double bond signals, also indicating successful polymerization and purification. The increasing BT-content series was normalized to 1181 cm<sup>-1</sup> (Figure 2). The signal at 1750

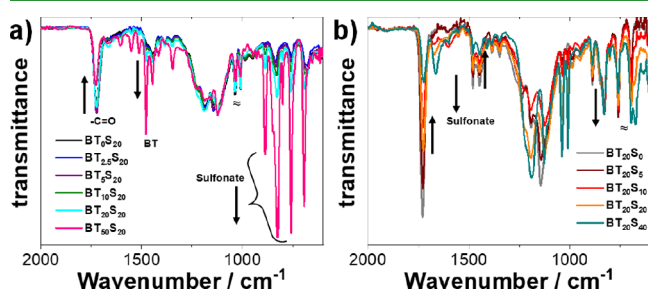


**Figure 2.** FTIR spectra of (a) **series 1** with increasing BT and (b) **series 2** with increasing S content. The spectra were normalized to significant peaks of the respective constant monomer.

cm<sup>-1</sup>, which corresponds to the carboxyl group of the methyl methacrylate, becomes less pronounced from BT<sub>0</sub>S<sub>20</sub> to BT<sub>50</sub>S<sub>20</sub>. The signal at 1500 cm<sup>-1</sup> and the majority of peaks in the fingerprint region increase within the series because they are attributable to the BT unit. The region between 1000 and 1250 cm<sup>-1</sup>, where concise signals from the sulfonate monomer can be expected, is comparatively unchanged over the samples of the first row. **Series 2** was normalized to the peak at 827 cm<sup>-1</sup> because the BT monomer content is expected to be constant. Again, the signal from the MMA decreases at 1750 cm<sup>-1</sup>, and signals corresponding to benzenesulfonate (1665 and 1000 to 1250 cm<sup>-1</sup>) increase in intensity. The FTIR spectra confirm the composition of the polymers and the trends of increasing BT monomer in **series 1** and increasing S monomer in **series 2**.

The structural and morphological characterization was extended by scanning electron microscopy (SEM) imaging of BT<sub>20</sub>S<sub>20</sub> as representative polymers (Figure S2, SI). SEM images show the typical irregular appearance of a cross-linked polymer. No structured porosity or ordered features could be observed. Thermogravimetric analysis (TGA) showed that the photocatalyst stayed intact up to 245 °C under air, comparable to previous data (Figure S3, SI).<sup>25</sup>

**Water Compatibility.** In the following, the dispersibility and water compatibility of the polymers in water was assessed.

In a simple experiment, all samples were dispersed in water using ultrasonication and examined after a rest period (Figure 3). In **series 1**, BT<sub>20</sub>S<sub>20</sub> and BT<sub>50</sub>S<sub>20</sub> appeared to be the most

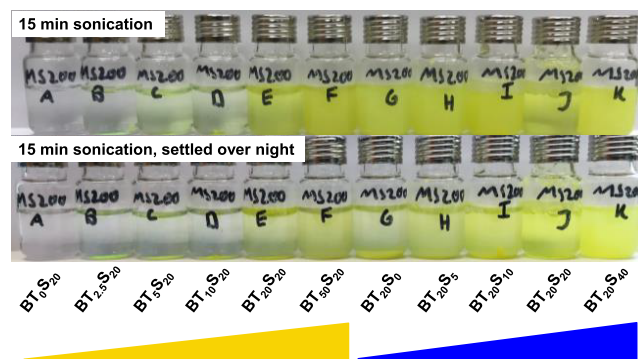


**Figure 3.** Qualitative dispersibility experiment. Polymers (5 mg/mL) were dispersed in water through ultrasonication (15 min) and left overnight for settling.

dispersible ones. Even after the rest period, there are still noticeable particles distributed in the liquid. In **series 2**, with increasing S content, the dispersibility in water increases. For BT<sub>20</sub>S<sub>20</sub> and BT<sub>20</sub>S<sub>50</sub>, no material settles at the bottom of the vials.

The observations made could be confirmed by a DFT-based estimation of hydration enthalpies. By subdividing the polymers into fragments, incremental hydration enthalpies can be calculated, and the tendency to dispersion and compatibility in the aqueous medium can be approximated (Figure S4, SI). Secondary entropic solubility effects resulting from the mobility of the chains, polymer rigidity, and structural organization of water around the solutes are neglected. In **series 1** with increasing BT content, the enthalpy of hydration increases slightly (Figure 4a). BT<sub>40</sub>S<sub>20</sub> should have the highest enthalpy of hydration. This is consistent with the dispersion experiment, where a slightly increase in solubility can be observed within the series. In **series 2** with increasing S content, the enthalpy of hydration increases strongly. This is

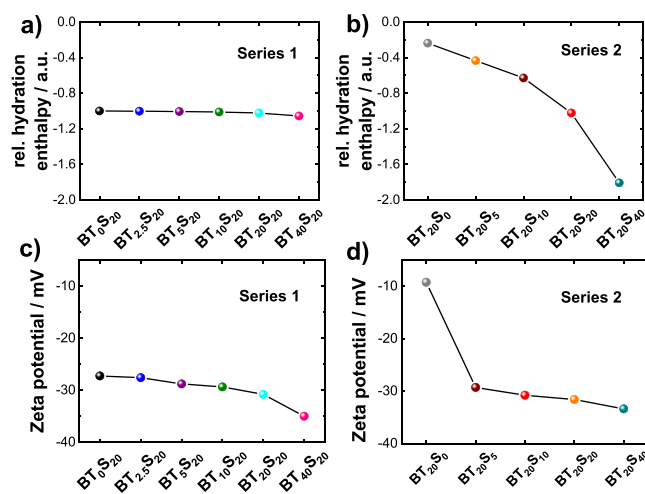


**Figure 4.** Calculated relative hydration enthalpies in (a) **series 1** with increasing BT content, (b) **series 2** with increasing S content, zeta potentials of (c) **series 1** and (d) **series 2**. Measurements with a polymer concentration of 0.5 mg/mL performed in 10<sup>-3</sup> M potassium chloride solution at pH 6.8 and 25 °C.

also consistent with the dispersion experiment, where an increase in solubility from almost insoluble ( $BT_{20}S_0$ ) to fully dispersed over several hours ( $BT_{20}S_{40}$ ) can be observed. The calculations emphasize that the solubility and dispersibility are largely determined by the sulfonate content and modulated by the BT content.

Zeta potential measurements were performed to draw further conclusions on water compatibility and electrostatic stabilization of the polymers in water. In both series, the magnitude of the electric potential grows with increase in BT and S monomers, respectively (Figure 4c, d). The resulting increase in stabilization and water compatibility by surface charges is consistent with the previously observed trend.  $BT_{20}S_0$  represents the only sample that, because of the absence of sulfonate comonomers, exhibits little electrokinetic potential in its dispersion.

In order to characterize the electro-optic properties of the polymers, UV/vis absorption spectroscopy, photoluminescence (PL), and time-resolved photoluminescence spectra (TRPL) were measured. For the PL spectra, the polymers were excited at their absorption maximum. For the TRPL measurements, the samples were excited at  $\lambda_{exc} = 380$  nm, and the decay was detected at the emission maximum. All copolymers were dispersed in water and measured in a glass cuvette. The UV/vis absorption spectra of the  $BT_0S_{20}$  to  $BT_{50}S_{20}$  series are shown in Figure 5a. With increasing BT content, it can be observed that the absorption maximum remains comparatively constant (Figure 5b). However, the absorption maximum shifts noticeably to about 404 nm at particularly high BT contents in sample  $BT_{50}S_{20}$ . When

observing the polymers' PL behavior, a red shift of the emission maximum was observed as the BT content in the series increased (Figure 5c, d). The lifetime of excited charge carriers was investigated by TRPL measurement (Figure 5e, f). With increasing BT content, the lifetime decreases from 5.6 ns for  $BT_{2.5}S_{20}$  to 1.27 ns for  $BT_{40}S_{20}$ .

**Optical and Electronic Properties.** By increasing the BT content, the average distance between two photoactive units is reduced. However, light absorption is independent of the ratio of the photoactive moiety to the other monomers because the electronic configuration in the ground state is not affected by changing the chemical composition of the polymers. Only at extremely high concentrations, where a large fraction of BT units is adjacent to BT units, an overlap of the  $\pi$ -systems occurs and results in a red shift of the absorption. In the excited state, energy transfers to neighboring BT units become more likely as BT content increases. In the case of direct proximity, electron transfers due to overlapping electron densities and the extension of delocalization are also conceivable. Both mechanisms lead to energy losses and shift the PL emission maximum to higher wavelengths. This effect is also evident when looking at the TRPL measurement results. The proximity of BT units and the associated transfer processes increase the number of possible decay mechanisms. With increasing BT content, the lifetime of charge carriers in the excited state decreases significantly.

The absorption spectra of the copolymers for the series  $BT_{20}S_0$  to  $BT_{20}S_{40}$  are plotted in Figure 6a. With increasing sulfonate content, a shift of the absorption maximum to

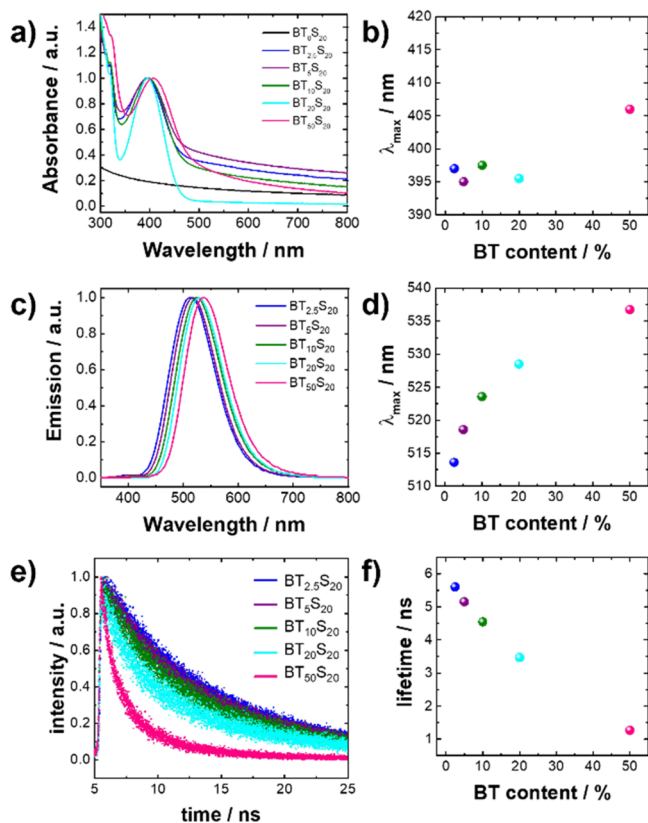


**Figure 5.** Comparison of (a) UV/vis, (b) absorption maxima, (c) PL spectra, (d) emission maxima, (e) TRPL measurements, and (f) excited-state lifetimes for series 1 from  $BT_{2.5}S_{20}$  to  $BT_{50}S_{20}$ .

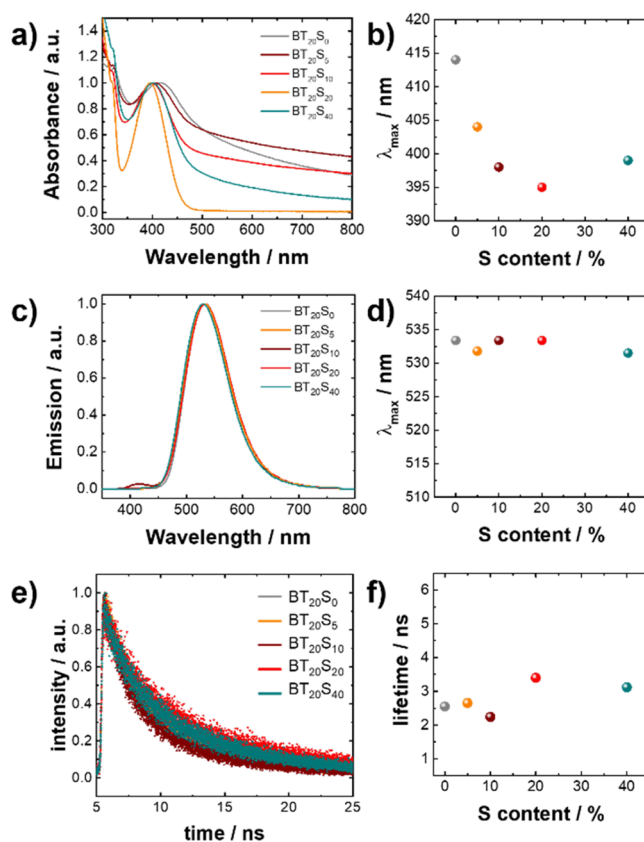


**Figure 6.** Comparison of (a) UV/vis, (b) absorption maxima, (c) PL spectra, (d) emission maxima, (e) TRPL measurements, and (f) excited state lifetimes for series 2 from  $BT_{20}S_0$  to  $BT_{20}S_{40}$ .

smaller wavelengths can be observed (Figure 6b). A minimum is reached for sample BT<sub>20</sub>S<sub>20</sub>. Toward sample BT<sub>20</sub>S<sub>40</sub>, the absorption wavelength again assumes a slightly higher value of 399 nm. The PL emission spectra of the sulfonate series are almost identical, and all have their maximum at 533 nm (Figure 6c, d). The lifetime of excited charge carriers was investigated by TRPL measurements (Figure 6e, f). With increasing S content, the lifetime does not change drastically. At low sulfonate ratios, the lifetimes are slightly lower than those for the higher content polymers.

In series 1, the position of the absorption maximum depends on the sulfonate content. We hypothesize that increased concentrations of negatively charged monomers in close proximity stabilize polar mesomeric states and partial charges. The ground-state energy levels of the photoactive moiety are lowered similar to a negative solvatochromic effect, and the absorption is blue-shifted. The emission spectra as well as the lifetimes of the excited charge carriers are independent of the sulfonate concentration. The BT concentration is sufficiently low, and interactions as well as transfer phenomena between the units play a minor role or are the same across all polymers. On a closer consideration, the slightly red-shifted emission maxima and shorter lifetimes of BT<sub>20</sub>S<sub>0</sub>, BT<sub>20</sub>S<sub>10</sub>, and BT<sub>20</sub>S<sub>20</sub> could be attributed to their solubility properties. Because of the lower sulfonate contents, the polymers are likely to be less swollen and the BT units are in closer spatial proximity. This could have similar quenching effects as in series 1 but in an attenuated form.

The electrooptical characterization was extended by cyclic voltammetry (CV) measurements of BT<sub>20</sub>S<sub>20</sub> as the representative polymer (Figure S5, SI). The data showed the lowest unoccupied molecular orbital (LUMO) to be  $-1.35$  V vs SCE. In combination with the Kubelka–Munk-transformed UV/vis spectrum, which gives a band gap of 2.83 eV, the highest occupied molecular orbital (HOMO) can be determined to be  $+1.48$  V vs SCE (Figure S5, SI). The values correspond to literature examples and can be directly derived from the small molecular catalyst 4,7-diphenylbenzothiadiazole (BTP<sub>h2</sub>).<sup>12,25,26</sup>

**Photocatalysis.** Persistent organic pollutants are not only stable in natural waters but also traceable in animal and plant organisms over long periods of time.<sup>27–29</sup> Although the contaminants pose a major health risk and have been the subject of political action at the global level for decades, numerous toxins are detectable at high concentrations in groundwaters.<sup>6,30,31</sup> Several strategies have been reported for pollutant removal, such as adsorption,<sup>32</sup> membrane separation,<sup>33</sup> microbial degradation,<sup>34</sup> advanced oxidation, enzymatic degradation, and so forth.<sup>35</sup> Some of these methods were hindered by disadvantages like high costs, long process time, secondary pollution, and poor operability. Compared to these methods, pure organic heterogeneous photocatalysts are particularly attractive for wastewater treatment because of its clear advantage in terms of easy operation and the use environment-friendly materials.<sup>36–38</sup> Therefore, the photocatalytic remediation of harmful organic compounds is of particular relevance.

For the kinetic comparison of the photocatalytic activity of the polymers, the degradation of 2,4-dichlorophenol (2,4-DCP) was chosen. The concentrations were assessed by using 4-*tert*-butyltoluene as the internal standard. In the series from BT<sub>0</sub>S<sub>20</sub> to BT<sub>40</sub>S<sub>20</sub>, BT<sub>20</sub>S<sub>20</sub> was found to be the most efficient catalyst by reducing the initial concentration to 12% after 4 h

(Figure 7a). Without benzothiadiazole units, the polymer was not showing conversion of the target compound (BT<sub>0</sub>S<sub>20</sub>).

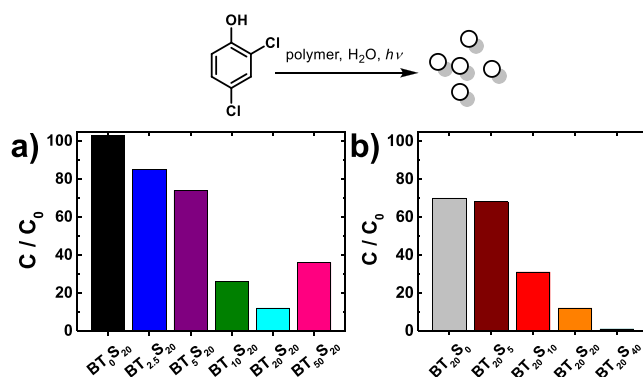


**Figure 7.** Bar diagrams for the photocatalytic degradation of 2,4-dichlorophenol by (a) series 1 and (b) series 2.

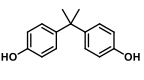
According to our previous work and other related studies, we believe that O<sub>2</sub><sup>•-</sup>, OH, and photoinduced holes participated in the reaction.<sup>39–43</sup> In particular, the degradation process can be divided into three steps referred to dehydroxylation, dechlorination, and benzene ring opening. In the first stage, 2,4-DCP was oxidized by OH, O<sub>2</sub><sup>•-</sup>, and photogenerated holes, forming dechlorinated and dehydroxylated intermediates as 2-chloro-1,4-benzenediol, 2-chlorophenol, and 4-chlorophenol or 4,6-dichloro-1,3-benzenediol. These species were then further converted to small molecular organics such as catechol, benzoquinone, and phenol and further broken into acids and finally converted to CO<sub>2</sub> and H<sub>2</sub>O. The photocatalytic activity increases from BT<sub>0</sub>S<sub>20</sub> to BT<sub>20</sub>S<sub>20</sub> and decreases again for BT<sub>40</sub>S<sub>20</sub>. Among the factors promoting higher conversion are the gradual increase in the amount of the photoactive moiety and the improved water solubility within the series. Increasing the BT content to BT<sub>40</sub>S<sub>20</sub> does not seem to have any further positive effect. As shown in the electro-optical characterization, high BT levels seem to contribute to charge carrier quenching and to the fundamental change of the  $\pi$ -electronic constitution of the photoactive units.

The photocatalytic polymer BT<sub>20</sub>S<sub>20</sub> was finally tested for repeating experiments to demonstrate its reusability. The experiments showed that BT<sub>20</sub>S<sub>20</sub> could be reused for degradation of 2,4-DCP for several cycles without suffering conversion and degradation rates (Figure S6, SI).

In series 2, the photocatalytic activity increased from BT<sub>20</sub>S<sub>0</sub> to BT<sub>20</sub>S<sub>40</sub>. BT<sub>20</sub>S<sub>40</sub> was found to be the most efficient catalyst by reducing the initial concentration to <1% after 4 h (Figure 7b). As it can be seen from sample BT<sub>20</sub>S<sub>0</sub>, the polarity and dispersibility without the sulfonate unit is sufficient to catalyze the degradation reaction. The photocatalytic activity gradually increases from BT<sub>20</sub>S<sub>0</sub> to BT<sub>20</sub>S<sub>40</sub>. Because PL and TRPL data do not indicate any significant change in photophysical properties within the series, the gradual increase in the sulfonate content and water compatibility seems to be mainly responsible for the activity of the polymers. The changing optical absorption does not seem to have a significant effect because the photocatalytic activity does not follow the absorption trend. The series emphasizes the concept of increasing activity in aqueous medium by copolymerization of charged monomers.

The reaction scope could be extended by the degradation of further substances with the photocatalyst BT<sub>20</sub>S<sub>20</sub>. The plastic

degradation products such as diethyl phthalate, acetophenone, and bisphenol-A were degraded efficiently and underline the versatility of the system (Figure 8).

pollutants			
initial concentration ( $n_0$ )	523 $\mu\text{mol}$	122 $\mu\text{mol}$	13 $\mu\text{mol}$
concentration after 4h ( $n_4$ )	3.3 $\mu\text{mol}$	116 $\mu\text{mol}$	0 $\mu\text{mol}$
degradation rate	122 $\mu\text{mol/h}$	1.5 $\mu\text{mol/h}$	3.3 $\mu\text{mol/h}$

**Figure 8.** Photocatalytic degradation rates of other organic pollutants using BT<sub>20</sub>S<sub>20</sub>.

## CONCLUSIONS

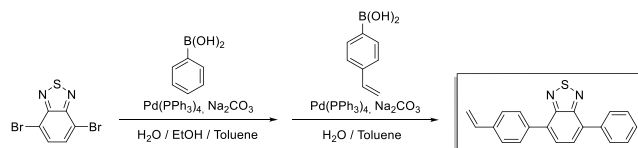
In summary, we developed a type of metal-free and redox active polymers for efficient photocatalytic remediation of organic pollutants in aqueous media. The radical copolymerization of charged sulfonate comonomers with MMA and benzothiadiazole enabled the further development of PMMA-based photocatalysts toward highly increased water compatibility. Using two series of polymers, one with increasing BT content and one with increasing sulfonate content, key structure–property relationships were elucidated. While increasing proportions of photoactive units strongly influence the photophysical properties due to proximity effects, the latter characteristics remain comparatively unchanged when altering the levels of solvent-mediating monomers. Kinetic studies of the 2,4-dichlorophenol degradation in water showed a polymer composition and solubility optimum for the photocatalytic reactivity. The reaction scope could be expanded to include the remediation of further contaminants detected in groundwater analyses. The study contributes significantly to the understanding of future material design and enables balancing between monomer composition, catalyst properties, and photocatalytic efficiency.

## EXPERIMENTAL SECTION

**Materials and Methods.** All chemicals and solvents were purchased from commercial sources and used as received unless otherwise noted. UV–vis absorption and fluorescence spectra were recorded on an Agilent Cary 60 spectrophotometer and a J&M TIDAS spectrofluorometer at ambient temperature, respectively. CV measurements were carried out on a Metrohm Autolab PGSTAT204 potentiostat/galvanostat with a three-electrode-cell system: a glassy carbon electrode as the working electrode, a Hg/HgCl<sub>2</sub> electrode as the reference electrode, a platinum wire as the counter electrode, and Bu<sub>4</sub>NPF<sub>6</sub> (0.1 M in acetonitrile) as the electrolyte. The scan rate was 100 mV s<sup>-1</sup> in the range of -1 to -2 eV. Gas chromatography–mass spectrometry (GC–MS) measurements were performed on a Shimadzu GC-2010 plus gas chromatograph with a QP2010 ultra mass spectrometer. The system operates with a fused silica column (Phenomenex, Zebron 5-ms nonpolar) and a flame ionization detector. <sup>1</sup>H and <sup>13</sup>C NMR spectra for all compounds were measured using a Bruker Avance 300 MHz. Solid-state <sup>13</sup>C CP MAS NMR measurements were carried out using a Bruker Avance II solid-state NMR spectrometer operating at 300 MHz Larmor frequency. The system is equipped with a standard 4 mm magic angle spinning (MAS) double resonance probe head. FTIR measurements were conducted with a Varian 1000 FTIR spectrometer. The morphology was investigated with a LEO Gemini 1530 scanning electron microscope. Thermogravimetric analysis (TGA) was conducted in an air atmosphere with temperature increasing from room temperature to 900 °C at a rate of

10 K/min. All DFT calculations were carried out with the Gaussian 09 package.<sup>44</sup> The structures were optimized at the B3LYP level of theory,<sup>45</sup> with the basis set of 6-31G(d).<sup>46,47</sup> The hydration calculations were performed together with the PCM (Polarizable Continuum Model) model by employing water as the solvent.<sup>48–50</sup> Zeta potential measurements were performed in 10<sup>-3</sup> M potassium chloride solution at pH 6.8 and 25 °C with a Malvern Zeta sizer (Malvern Instruments, UK). Time-resolved PL spectroscopy (TRPL)/time-correlated single-photon counting (TCSPC) measurements were conducted with a FluoTime200 time-correlated single-photon counting setup. Samples were excited with a laser at 380 nm, which was controlled by PicoQuant PDL 800-D. The signal was detected using a microchannel plate photomultiplier tube that was connected to a PicoHarp 300 time-correlated single-photon counting system. The instrument response function was measured using a dispersion of silica nanoparticles (LUDOX HS-40 colloidal silica) in water.

### Monomer Synthesis.



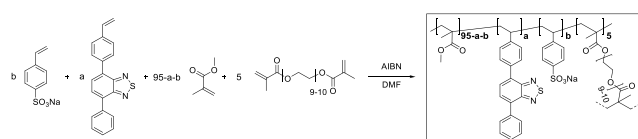
Step 1. (4-Bromo-7-phenylbenzo[*c*][1,2,5]thiadiazole): phenylboronic acid (899 mg, 7.37 mmol, 1.00 equiv), 4,7-dibromobenzo[*c*][1,2,5]thiadiazole (3.25 g, 11.06 mmol, 1.50 equiv), toluene (30 mL), aqueous Na<sub>2</sub>CO<sub>3</sub> solution (2 M, 12.4 mL), and ethanol (12.4 mL) were placed in a 100 mL Schlenk flask. After degassing by Ar bubbling for 20 min, Pd(PPh<sub>3</sub>)<sub>4</sub> (254 mg, 220  $\mu\text{mol}$ , 0.03 equiv) was added in an Ar counter stream. The solution was vigorously stirred at 90 °C for 48 h. After cooling to room temperature, the resulting mixture was extracted with dichloromethane (4 × 40 mL). The combined organic phases were washed with brine (100 mL) and dried over anhydrous MgSO<sub>4</sub>. After filtration and rotary evaporation of solvents, the residue was purified by column chromatography on silica gel (petroleum ether/dichloromethane 3:1). The light green solid (2.4 g) was used as is in the next step.

Step 2. (4-Phenyl-7-(4-vinylphenyl)benzo[*c*][1,2,5]thiadiazole): the crude product from step 1 (2.4 g), (4-vinylphenyl)boronic acid (1.59 g, 10.75 mmol, 1.3 equiv), toluene (22 mL), and aqueous Na<sub>2</sub>CO<sub>3</sub> solution (2 M, 12 mL) were combined in a 100 mL Schlenk tube. After degassing by Ar bubbling for 20 min, Pd(PPh<sub>3</sub>)<sub>4</sub> (190 mg, 165  $\mu\text{mol}$ , 0.02 equiv) was added in an Ar counter stream. The solution was vigorously stirred at 90 °C for 48 h. After cooling to room temperature, water was added (55 mL), and the resulting mixture was extracted with dichloromethane (4 × 40 mL). The combined organic phases were washed with 1 M NaOH (70 mL) and brine (70 mL). After drying over anhydrous MgSO<sub>4</sub> and filtration, rotary evaporation yielded the crude product. The residue was purified by column chromatography on silica gel (petroleum ether/DCM 1:0 → 0:1). The product was obtained as bright yellow powder (1.76 g).

<sup>1</sup>H NMR (300 MHz, CDCl<sub>3</sub>)  $\delta$  7.98 (d, 4H), 7.80 (s, 2H), 7.61–7.44 (m, 4H), 6.82 (q, 1H), 5.86 (d, 1H), 5.34 (d, 1H).

<sup>13</sup>C NMR (75 MHz, CDCl<sub>3</sub>)  $\delta$  154.27, 154.21, 137.78, 137.56, 136.91, 136.53, 133.50, 133.05, 129.52, 129.38, 128.77, 128.52, 128.27, 127.99, 126.61, 114.67.

### Polymer Synthesis.



4-Phenyl-7-(4-vinylphenyl)benzo[*c*][1,2,5]thiadiazole (0–0.5 equiv), methyl methacrylate (0.25–0.75 equiv), and poly-

ethylene glycol dimethacrylate (0.05 equiv) were charged in a vial and dissolved in DMF (3.6 mL). The solution was degassed with Ar for 5 min, and azobisisobutyronitrile (0.008 equiv) was added. Then, the vial was capped, and the solution was purged with Ar while stirring for 5 min. After heating to 70 °C overnight, the reaction was cooled to room temperature. The polymer was transferred with Milli Q water and dialyzed with THF/water (1:10) for 24 h (SnakeSkin dialysis tubing, 3.5 K MWCO, 2 mm, ThermoFisher). After 12 h, the solution was exchanged for fresh THF/water (1:10). The polymers were freeze-dried for 24 h under high vacuum and appeared as dry colorless to bright yellow solids.

**Photocatalysis Kinetics.** To obtain a saturated solution, 2,4-dichlorophenol (1.0 g, 6.14 mmol) was added to Milli Q water (50 mL). The suspension was stirred for 24 h at room temperature. After settling, the supernatant was collected and used as the stock solution for the kinetic experiments. In a 20 mL vial equipped with a magnetic stir bar, the polymer (10 mg) and stock solution (5 mL) were combined. After passing air through the setup for 2 min, the reaction was stirred for 30 min in the dark to rule out potential absorption of the small molecule on the organic polymer networks. A sample for GC–MS analysis was taken and used as the starting point (0 h). The vial was placed under irradiation of blue LEDs (60 mW/cm<sup>2</sup>) and stirred at room temperature for 4 h. Samples for GC–MS analysis were taken after 1, 2, and 4 h.

Every sample taken from the aqueous solution (0.2 mL) was extracted with DCM (1 mL). The organic phase was further used. 4-*tert*-Butyltoluene (PTBT) was added as the internal standard (0.33 mL in 1 mL of DCM stock solution, 10 μL of stock solution in every GC–MS vial).

For diethyl phthalate, acetophenone and bisphenol-A saturated aqueous solutions were obtained similarly. The further procedure followed the one described above. The degradation rate was determined using a sample taken after a reaction time of 4 h.

**Repeating Experiments.** To obtain a saturated solution, 2,4-dichlorophenol (1.0 g, 6.14 mmol) was added to Milli Q water (50 mL). The suspension was stirred for 24 h at room temperature. After settling, the supernatant was collected and used as the stock solution for experiments. In a 20 mL vial equipped with a magnetic stir bar, polymer (10 mg) and stock solution (5 mL) were combined. After passing air through the setup for 2 min, the reaction was stirred for 30 min in the dark to rule out potential absorption of the small molecule on the organic polymer networks. The vial was placed under irradiation of blue LEDs (60 mW/cm<sup>2</sup>) and stirred at room temperature for 4 h. After reaction, the polymer was collected by centrifugation, washed using Milli Q water five times, and dried using vacuum for the next cycle.

The reactant taken from the aqueous solution (0.2 mL) was extracted with DCM (1 mL). The organic phase was further used. 4-*tert*-Butyltoluene (PTBT) was added as the internal standard (0.33 mL in 1 mL of DCM stock solution, 10 μL of stock solution in every GC–MS vial).

## ■ ASSOCIATED CONTENT

### SI Supporting Information

The Supporting Information is available free of charge at <https://pubs.acs.org/doi/10.1021/acsapm.2c00688>.

More details of monomer characterizations, theoretical calculations, and repeating experiments etc. (PDF)

## ■ AUTHOR INFORMATION

### Corresponding Author

Kai A. I. Zhang – Max Planck institute for Polymer Research, 55128 Mainz, Germany; Department of Materials Science, Fudan University, Shanghai 200433, P. R. China;

orcid.org/0000-0003-0816-5718; Email: kai.zhang@mpip-mainz.mpg.de, kai\_zhang@fudan.edu.cn

### Authors

Niklas Huber – Max Planck institute for Polymer Research, 55128 Mainz, Germany

Masis Sirim – Max Planck institute for Polymer Research, 55128 Mainz, Germany

Zhuangfei Qian – Department of Materials Science, Fudan University, Shanghai 200433, P. R. China

Calum T. J. Ferguson – Max Planck institute for Polymer Research, 55128 Mainz, Germany; School of Chemistry, University of Birmingham, Birmingham B15 2TT, U.K.; orcid.org/0000-0002-6168-4624

Wenxin Wei – Department of Materials Science, Fudan University, Shanghai 200433, P. R. China

Complete contact information is available at: <https://pubs.acs.org/10.1021/acsapm.2c00688>

### Funding

Open access funded by Max Planck Society.

### Notes

The authors declare no competing financial interest.

## ■ ACKNOWLEDGMENTS

The authors thank Prof. Katharina Landfester for fruitful discussion and support. N.H. acknowledges the Kekulé fellowship of Fonds der chemischen Industrie (FCI) and the fellowship of the Gutenberg-Akademie of the Johannes Gutenberg University of Mainz. This work is part of the research conducted by the MaxSynBio consortium that is jointly funded by the Federal Ministry of Education and Research of Germany (BMBF) and the Max Planck Society (MPG) (Grant No. 031A359A). K.A.I.Z. acknowledges the National Natural Science Foundation of China (Grant No. 52173198) for funding.

## ■ REFERENCES

- (1) Tachibana, Y.; Vayssieres, L.; Durrant, J. R. Artificial photosynthesis for solar water-splitting. *Nat. Photonics* **2012**, *6*, 511–518.
- (2) Nagib, D. A.; MacMillan, D. W. C. Trifluoromethylation of arenes and heteroarenes by means of photoredox catalysis. *Nature* **2011**, *480*, 224–228.
- (3) Ghosh, S.; Kouame, N. A.; Ramos, L.; Remita, S.; Dazzi, A.; Deniset-Besseau, A.; Beaunier, P.; Goubard, F.; Aubert, P.-H.; Remita, H. Conducting polymer nanostructures for photocatalysis under visible light. *Nat. Mater.* **2015**, *14*, 505–511.
- (4) Zhao, C.; Chen, Z.; Shi, R.; Yang, X.; Zhang, T. Recent Advances in Conjugated Polymers for Visible-Light-Driven Water Splitting. *Adv. Mater.* **2020**, *32*, No. e1907296.
- (5) Alfonsi, K.; Colberg, J.; Dunn, P. J.; Fevig, T.; Jennings, S.; Johnson, T. A.; Kleine, H. P.; Knight, C.; Nagy, M. A.; Perry, D. A. Green chemistry tools to influence a medicinal chemistry and research chemistry based organisation. *Green Chem.* **2008**, *10*, 31–36.
- (6) Weber, R.; Watson, A.; Forter, M.; Oliaei, F. Persistent organic pollutants and landfills—a review of past experiences and future challenges. *Waste Manage. Res.* **2011**, *29*, 107–121.
- (7) Ferguson, C. T. J.; Huber, N.; Kuckhoff, T.; Zhang, K. A. I.; Landfester, K. Dispersible porous classical polymer photocatalysts for visible light-mediated production of pharmaceutically relevant compounds in multiple solvents. *J. Mater. Chem. A* **2020**, *8*, 1072–1076.
- (8) Ferguson, C. T. J.; Zhang, K. A. I. Classical Polymers as Highly Tunable and Designable Heterogeneous Photocatalysts. *ACS Catal.* **2021**, *11*, 9547–9560.

- (9) Kuckhoff, T.; Landfester, K.; Zhang, K. A. I.; Ferguson, C. T. J. Photocatalytic Hydrogels with a High Transmission Polymer Network for Pollutant Remediation. *Chem. Mater.* **2021**, *33*, 9131–9138.
- (10) Boussiron, C.; Le Behec, M.; Petrizza, L.; Sabalot, J.; Lacombe, S.; Save, M. Synthesis of Film-Forming Photoactive Latex Particles by Emulsion Polymerization-Induced Self-Assembly to Produce Singlet Oxygen. *Macromol. Rapid Commun.* **2019**, *40*, No. 1800329.
- (11) Tobin, J. M.; McCabe, T. J.; Prentice, A. W.; Holzer, S.; Lloyd, G. O.; Paterson, M. J.; Arrighi, V.; Cormack, P. A.; Vilela, F. Polymer-supported photosensitizers for oxidative organic transformations in flow and under visible light irradiation. *ACS Catal.* **2017**, *7*, 4602–4612.
- (12) Wang, L.; Byun, J.; Li, R.; Huang, W.; Zhang, K. A. I. Molecular Design of Donor-Acceptor-Type Organic Photocatalysts for Metal-free Aromatic C-C Bond Formations under Visible Light. *Adv. Synth. Catal.* **2018**, *360*, 4312–4318.
- (13) Brink, G.-J. T.; Arends, I. W. C. E.; Sheldon, R. A. Green, Catalytic Oxidation of Alcohols in Water. *Science* **2000**, *287*, 1636–1639.
- (14) Wang, X. C.; Maeda, K.; Thomas, A.; Takanebe, K.; Xin, G.; Carlsson, J. M.; Domen, K.; Antonietti, M. A metal-free polymeric photocatalyst for hydrogen production from water under visible light. *Nat. Mater.* **2009**, *8*, 76–80.
- (15) Wang, L.; Fernandez-Teran, R.; Zhang, L.; Fernandes, D. L.; Tian, L.; Chen, H.; Tian, H. Organic Polymer Dots as Photocatalysts for Visible Light-Driven Hydrogen Generation. *Angew. Chem., Int. Ed.* **2016**, *55*, 12306–12310.
- (16) Pati, P. B.; Damas, G.; Tian, L.; Fernandes, D. L.; Zhang, L.; Pehlivan, I. B.; Edvinsson, T.; Araujo, C. M.; Tian, H. An experimental and theoretical study of an efficient polymer nano-photocatalyst for hydrogen evolution. *Energy Environ. Sci.* **2017**, *10*, 1372–1376.
- (17) Ma, B. C.; Ghasimi, S.; Landfester, K.; Zhang, K. A. Enhanced visible light promoted antibacterial efficiency of conjugated microporous polymer nanoparticles via molecular doping. *J. Mater. Chem. B* **2016**, *4*, 5112–5118.
- (18) Jiang, S.; Ma, B. C.; Huang, W.; Kaltbeitzel, A.; Kizisavas, G.; Crespy, D.; Zhang, K. A.; Landfester, K. Visible light active nanofibrous membrane for antibacterial wound dressing. *Nanoscale Horiz.* **2018**, *3*, 439–446.
- (19) Zhu, C.; Liu, L.; Yang, Q.; Lv, F.; Wang, S. Water-Soluble Conjugated Polymers for Imaging, Diagnosis, and Therapy. *Chem. Rev.* **2012**, *112*, 4687–4735.
- (20) Ghasimi, S.; Prescher, S.; Wang, Z. J.; Landfester, K.; Yuan, J.; Zhang, K. A. I. Heterophase Photocatalysts from Water-Soluble Conjugated Polyelectrolytes: An Example of Self-Initiation under Visible Light. *Angew. Chem., Int. Ed.* **2015**, *54*, 14549–14553.
- (21) Byun, J.; Huang, W.; Wang, D.; Li, R.; Zhang, K. A. CO<sub>2</sub>-Triggered switchable hydrophilicity of a heterogeneous conjugated polymer photocatalyst for enhanced catalytic activity in water. *Angew. Chem., Int. Ed.* **2018**, *57*, 2967–2971.
- (22) Dawson, R.; Laybourn, A.; Clowes, R.; Khimiyak, Y. Z.; Adams, D. J.; Cooper, A. I. Functionalized conjugated microporous polymers. *Macromolecules* **2009**, *42*, 8809–8816.
- (23) Urakami, H.; Zhang, K.; Vilela, F. Modification of conjugated microporous poly-benzothiadiazole for photosensitized singlet oxygen generation in water. *Chem. Commun.* **2013**, *49*, 2353–2355.
- (24) Ghasimi, S.; Landfester, K.; Zhang, K. A. Water Compatible Conjugated Microporous Polyazulene Networks as Visible-Light Photocatalysts in Aqueous Medium. *ChemCatChem* **2016**, *8*, 694–698.
- (25) Huber, N.; Li, R.; Ferguson, C. T.; Gehrig, D. W.; Ramanan, C.; Blom, P. W.; Landfester, K.; Zhang, K. A. A PMMA-based heterogeneous photocatalyst for visible light-promoted [4+ 2] cycloaddition. *Catal. Sci. Technol.* **2020**, *10*, 2092–2099.
- (26) Ferguson, C. T. J.; Huber, N.; Landfester, K.; Zhang, K. A. I. Dual-Responsive Photocatalytic Polymer Nanogels. *Angew. Chem., Int. Ed.* **2019**, *58*, 10567–10571.
- (27) Marin, M. L.; Santos-Juanes, L.; Arques, A.; Amat, A. M.; Miranda, M. A. Organic Photocatalysts for the Oxidation of Pollutants and Model Compounds. *Chem. Rev.* **2012**, *112*, 1710–1750.
- (28) Zheng, Q.; Durkin, D. P.; Elenewski, J. E.; Sun, Y.; Banek, N. A.; Hua, L.; Chen, H.; Wagner, M. J.; Zhang, W.; Shuai, D. Visible-Light-Responsive Graphitic Carbon Nitride: Rational Design and Photocatalytic Applications for Water Treatment. *Environ. Sci. Technol.* **2016**, *50*, 12938–12948.
- (29) Ahmed, S. N.; Haider, W. Heterogeneous photocatalysis and its potential applications in water and wastewater treatment: a review. *Nanotechnology* **2018**, *29*, 342001.
- (30) Buccini, J. The development of a global treaty on persistent organic pollutants (POPs). In *Persistent organic pollutants*; Springer: Berlin Heidelberg, 2003; pp 13–30.
- (31) Eggen, T.; Moeder, M.; Arukwe, A. Municipal landfill leachates: a significant source for new and emerging pollutants. *Sci. Total Environ.* **2010**, *408*, 5147–5157.
- (32) Ezung, S. L.; Baruah, M.; Supong, A.; Sharma, S.; Sinha, D. Experimental and theoretical insight into the adsorption of 2,4-dichlorophenol on low-cost bamboo sheath activated carbon. *Sustain. Chem. Pharm.* **2022**, *26*, No. 100643.
- (33) Yang, X.; Huang, J.; Yang, F.; Wang, W.; Xue, C.; Zhou, W.; Wu, Y.; Shao, L.; Zhang, Y. Metal-organophosphate biphasic interfacial coordination reaction synthesizing nanofiltration membranes with the ultrathin selective layer, excellent acid-resistance and antifouling performance. *J. Membr. Sci.* **2022**, *653*, No. 120521.
- (34) Zhang, G. Treatment of aqueous pentachlorophenol by horseradish peroxidase and hydrogen peroxide. *Water Res.* **2000**, *34*, 1629–1637.
- (35) Masuda, M.; Sakurai, A.; Sakakibara, M. Effect of reaction conditions on phenol removal by polymerization and precipitation using *Coprinus cinereus* peroxidase. *Enzyme Microb. Technol.* **2001**, *28*, 295–300.
- (36) Huang, Q.; Cao, M.; Ai, Z.; Zhang, L. Reactive oxygen species dependent degradation pathway of 4-chlorophenol with Fe@Fe<sub>2</sub>O<sub>3</sub> core-shell nanowires. *Appl. Catal., B* **2015**, *162*, 319–326.
- (37) Zhao, W.; Ma, W.; Chen, C.; Zhao, J.; Shuai, Z. Efficient degradation of toxic organic pollutants with Ni<sub>2</sub>O<sub>3</sub>/TiO<sub>2</sub>(2-x)Bx under visible irradiation. *J. Am. Chem. Soc.* **2004**, *126*, 4782–4783.
- (38) Zhu, Q.; Sun, Y.; Xu, S.; Li, Y.; Lin, X.; Qin, Y. Rational design of 3D/2D In<sub>2</sub>O<sub>3</sub> nanocube/ZnIn<sub>2</sub>S<sub>4</sub> nanosheet heterojunction photocatalyst with large-area “high-speed channels” for photocatalytic oxidation of 2,4-dichlorophenol under visible light. *J. Hazard. Mater.* **2020**, *382*, No. 121098.
- (39) Li, R.; Byun, J.; Huang, W.; Ayed, C.; Wang, L.; Zhang, K. A. I. Poly(benzothiadiazoles) and Their Derivatives as Heterogeneous Photocatalysts for Visible-Light-Driven Chemical Transformations. *ACS Catal.* **2018**, *8*, 4735–4750.
- (40) Ortega-Liebana, M. C.; Hueso, J. L.; Ferdousi, S.; Arenal, R.; Irusta, S.; Yeung, K. L.; Santamaria, J. Extraordinary sensitizing effect of co-doped carbon nanodots derived from mate herb: Application to enhanced photocatalytic degradation of chlorinated wastewater compounds under visible light. *Appl. Catal., B* **2017**, *218*, 68–79.
- (41) Xu, L.; Wang, J. Fenton-like degradation of 2,4-dichlorophenol using Fe<sub>3</sub>O<sub>4</sub> magnetic nanoparticles. *Appl. Catal., B* **2012**, *123–124*, 117–126.
- (42) Ayed, C.; Caire da Silva, L.; Wang, D.; Zhang, K. A. I., Designing conjugated microporous polymers for visible light-promoted photocatalytic carbon-carbon double bond cleavage in aqueous medium. *J. Mater. Chem. A* **2018**, *6*, 22145–22151.
- (43) Rakibuddin, M.; Ananthakrishnan, R. Effective photocatalytic dechlorination of 2,4-dichlorophenol by a novel graphene encapsulated ZnO/Co<sub>3</sub>O<sub>4</sub> core-shell hybrid under visible light. *Photochem. Photobiol. Sci.* **2016**, *15*, 86–98.
- (44) M. J., Frisch; G. W., Trucks; H. B., Schlegel; G. E., Scuseria; M. A., Robb; J. R., Cheeseman; G., Scalmani; V., Barone; G. A., Petersson; H., Nakatsuji; X., Li; M., Caricato; A., Marenich; J., Bloino; B. G., Janesko; R., Gomperts; B., Mennucci; H. P., Hratchian; J. V., Ortiz; A. F., Izmaylov; J. L., Sonnenberg; D., Williams-Young; F.,

Ding; F., Lipparini; F., Egidi; J., Goings; B., Peng; A., Petrone; T., Henderson; D., Ranasinghe; V. G., Zakrzewski; J., Gao; N., Rega; G., Zheng; W., Liang; M., Hada; M., Ehara; K., Toyota; R., Fukuda; J., Hasegawa; M., Ishida; T., Nakajima; Y., Honda; O., Kitao; H., Nakai; T., Vreven; K., Throssell; J. A., Montgomery, Jr.; J. E., Peralta; F., Ogliaro; M., Bearpark; J. J., Heyd; E., Brothers; K. N., Kudin; V. N., Staroverov; T., Keith; R., Kobayashi; J., Normand; K., Raghavachari; A., Rendell; J. C., Burant; S. S., Iyengar; J., Tomasi; M., Cossi; J. M., Millam; M., Klene; C., Adamo; R., Cammi; J. W., Ochterski; R. L., Martin; K., Morokuma; O., Farkas; J. B., Foresman; Fox, D. J. *Gaussian 09, revision A. 02*; Gaussian, Inc.: Wallingford CT, 2009.

(45) Becke, A. D. Density-functional thermochemistry. III. The role of exact exchange. *J. Chem. Phys.* **1993**, *98*, 5648–5652.

(46) Clark, T.; Chandrasekhar, J.; Spitznagel, G. W.; Schleyer, P. V. Efficient Diffuse Function-Augmented Basis Sets for Anion Calculations. Iii. The 3-21+G Basis Set for First-Row Elements, Li-F. *J. Comput. Chem.* **1983**, *4*, 294–301.

(47) McLean, A. D.; Chandler, G. S. Contracted Gaussian-Basis Sets for Molecular Calculations. I. 2nd Row Atoms, Z=11-18. *J. Chem. Phys.* **1980**, *72*, 5639–5648.

(48) Miertuš, S.; Scrocco, E.; Tomasi, J. Electrostatic interaction of a solute with a continuum. A direct utilization of AB initio molecular potentials for the prevision of solvent effects. *Chem. Phys.* **1981**, *55*, 117–129.

(49) Miertus, S.; Tomasi, J. Approximate evaluations of the electrostatic free energy and internal energy changes in solution processes. *Chem. Phys.* **1982**, *65*, 239–245.

(50) Pascual-Ahuir, J.-L.; Silla, E.; Tunon, I. GEPOL: An improved description of molecular surfaces. III. A new algorithm for the computation of a solvent-excluding surface. *J. Comput. Chem.* **1994**, *15*, 1127–1138.

## Recommended by ACS

### Backbone Degradation of Polymethacrylates via Metal-Free Ambient-Temperature Photoinduced Single-Electron Transfer

John B. Garrison, Brent S. Sumerlin, *et al.*

MARCH 15, 2022  
ACS MACRO LETTERS

READ [↗](#)

### Closed-Loop Recyclable Aliphatic Poly(ester-amide)s with Tunable Mechanical Properties

Yu-Ting Guo, Zi-Chen Li, *et al.*

MAY 10, 2022  
MACROMOLECULES

READ [↗](#)

### Water Repellency of Bottlebrush Polymers Consisting of Monomer Units with a Long Alkyl Chain Synthesized by Ru-Catalyzed Living Radical Polymerization

Nobuo Murase, Takuma Kawabe, *et al.*

NOVEMBER 01, 2019  
ACS APPLIED POLYMER MATERIALS

READ [↗](#)

### Highly Stretchable, Ultratough, and Strong Polyesters with Improved Postcrystallization Optical Property Enabled by Dynamic Multiple Hydrogen Bonds

Shuai Sun, Yongping Bai, *et al.*

JANUARY 22, 2021  
MACROMOLECULES

READ [↗](#)

Get More Suggestions >